Islamic University Journal of Applied Sciences (IUJAS)
https://journals.iu.edu.sa/jesc

Volume VII, Issue II, Dec 2025, Pages 226-247

Flow and Dispersion Characteristics Around Buildings: Numerical Evaluation

Mohammed Awdah B Alshehre, Wedad Hassan Asiri, Halemah Ibrahim Elsaeedy, Nejla Mahjoub Said *

Department of Physics, College of Science, King Khalid University, Abha 61413, Saudi Arabia

*Corresponding author: (Nejla Mahjoub Said), *Email Address*: **nalmahjoub@kku.edu.sa**

Abstract

Predicting gas dispersion from chimneys in urban environments is essential for minimizing impacts on air quality and human health. This study presents a numerical investigation of pollutant dispersion under turbulent flow, accounting for the influence of buildings and obstacles in a realistic industrial setting. Flow dynamics, heat transfer, and pollutant transport are analyzed to understand emission behavior in the near-field region. A parametric analysis examines the effects of chimney height, velocity ratios, and building placement. Results show that topography and structural features significantly alter wind patterns, pollutant concentration, and plume trajectory, particularly near ground and building levels. Chimney height proved the most critical factor: taller chimneys promoted wider diffusion before ground contact, whereas shorter ones caused plume looping and localized pollution. The findings support the design guideline that chimneys should be at least 2.5 times the height of nearby structures.

Keywords: Numerical simulation; Pollutant dispersion; chimney height; Turbulent flow; Plume looping; Built environment.

https://doi.org/10.63070/jesc.2025.033
Received 07 November 2025; Revised 27 November 2025; Accepted 05 December 2025.
Available online 10 December 2025.

1. Introduction

With rapid urbanization and industrial expansion, air pollution has become a major concern for organizations responsible for environmental protection. Understanding how pollutants disperse in urban areas is critical, since factors such as the source of emissions, building density, street geometry, and the relative position of obstacles strongly influence the dynamics of pollutant transport. Regulations often set discharge limits, but predicting pollutant behavior near buildings requires advanced tools.

In recent decades, Computational Fluid Dynamics (CFD) has become an essential approach for analyzing wind flow and pollutant dispersion in built environments. Numerous studies have assessed the reliability of CFD by comparing turbulence models with experimental data. For example, Tominaga and Stathopoulos [1, 2] evaluated different turbulence models, showing that the RNG k-ε and LES models provide better predictions of pollutant dispersion around buildings than standard models. Similarly, Gousseau et al. [3] demonstrated that both RANS and LES approaches can accurately capture pollutant dispersion from rooftop chimneys, particularly when the source is outside the recirculation zone.

Other works have focused on the influence of building geometry. Jiang and Yoshie [4], using LES, showed that reducing the aspect ratio of elevated buildings enhances vortex shedding and expands the recirculation region downstream. Rossi et al. [5, 6] applied direct numerical simulations to highlight the role of large-scale instabilities in altering plume mixing and dispersion scales. More recently, Yassin et al. [7] investigated rooftop chimney emissions under varying atmospheric conditions. Their results revealed that pollutant concentrations are highest near the stack, with stable conditions enhancing flow separation and unstable conditions promoting stronger vortex motion.

In parallel, Ben Ramoul et al. [8] studied pollutant dispersion around isolated and grouped buildings using different RANS turbulence models in Open FOAM. Their results, validated against wind tunnel experiments, confirmed that the RNG k-ε model offered the closest agreement with experimental data.

Overall, these studies emphasize the importance of turbulence modeling and building configuration in predicting pollutant dispersion. Yet, despite these advances, further research is required to explore realistic urban scenarios and optimize modeling approaches for reliable air quality assessments in complex environments.

Recent research has further highlighted the complex interactions between urban structures and airflow, which strongly influence pollutant dispersion in cities. Fu et al. [9] used a combination of Proper Orthogonal Decomposition (POD) and Dynamic Mode Decomposition (DMD) to identify dominant

flow structures in street canyons, highlighting how vortices and turbulent regions govern pollutant movement. Another study by Fu et al. [10] showed that turbulence model selection and building aspect ratios are critical for accurately simulating reactive pollutant dispersion around isolated structures. Huang et al. [11] revealed that even small rotations of high-rise buildings can deflect airflow, generate wake vortices, and shift pollutant plumes, demonstrating the importance of building orientation on near-ground air quality. Chen et al. [12] demonstrated that the spacing and arrangement of connected high-rise buildings significantly affect wind patterns, vortex formation, and recirculation zones, which in turn influence pollutant spread. Similarly, Quentin et al. [13] showed that tall buildings in Hanoi create recirculation zones and pressure-driven flows that either trap pollutants near the ground or lift them to higher layers, emphasizing the role of urban architecture in both horizontal and vertical pollutant transport. Together, these studies underline the importance of carefully considering building geometry, layout, orientation, and turbulence characteristics when modeling urban pollutant dispersion and designing healthier city environments.

Small-scale wind tunnel experiments offer a key advantage over field trials, as boundary conditions can be carefully controlled to match the problem under investigation. However, such tests are often limited by the number of measurement points, and even with advanced techniques like Particle Image Velocimetry (PIV) and Laser-Induced Fluorescence, issues such as laser light shielding in complex urban models may arise. Moreover, wind tunnel testing is expensive, time-consuming, and constrained by similarity requirements, particularly in buoyant flow studies.

Several studies have explored pollutant dispersion around buildings using both experimental and numerical approaches. Chávez et al. [14] examined pollutant dilution around isolated and grouped buildings under a perpendicular wind direction, while Lateb et al. [15] applied Computational Fluid Dynamics (CFD) with a realizable k-ε turbulence model to study pollutant dispersion from a roof stack in the wake of a tower, comparing full-scale and wind tunnel results with good agreement. Similarly, Liu et al. [16] investigated pollutant transport around a high-rise residential building in Hong Kong using a boundary-layer wind tunnel, with results later reproduced numerically by Zhang et al. [17]. These works confirmed differences in pollutant pathways for upwind and downwind emissions. More recently, Yu et al. [18] extended these investigations to various building shapes and wind incidence angles.

Together, these studies highlight the importance of combining wind tunnel experiments with CFD simulations to better capture the complex flow structures and pollutant dispersion patterns around buildings.

Air pollution levels are often higher in poorly ventilated areas, making it essential to understand the spatial distribution of pollutant concentrations for air quality management. Such studies require insight into both the turbulence of the surrounding environment and the flow dynamics altered by the presence of obstacles.

In this work, the mean flow field associated with pollutant dispersion from a full-scale industrial chimney under turbulent conditions is numerically investigated, extending modeling approaches to larger scales. The analysis considers the influence of wind velocity and chimney height on plume evolution. Three configurations are explored:

- Dispersion over terrain with a single obstacle,
- Dispersion over terrain with two obstacles of identical shape.

The first part examines how an isolated obstacle affects pollutant concentration at ground level and on the building roof. The second part focuses on pollutant dispersion in the presence of multiple obstacles, highlighting three key mechanisms: topological effects, wake-induced mixing, and flow blockage.

2. Computational set-up

The average flow field around the chimney and the obstacle fixed to a ground under turbulent flow is achieved by varying u_∞. A steady, three-dimensional and turbulent flow is taken into account. The numerical approach employed in the present study follows the methodology developed by Mahjoub et al. [19–122], as the model used has been validated by these authors. A chimney of height h and diameter d is considered, emitting a mixture of gases representative of the real case of a thermal power station: 20.9% carbon dioxide (CO_2), 76.9% nitrogen (N_2), 1.8% oxygen (O_2), 0.4% sulfur dioxide (SO_2), with an ejection velocity v_0 and at a temperature T_0 (110°C). This plume is subjected to a wind speed u_∞, the ambient temperature is T_∞ (18°C).

The laws of conservation of mass, moment and energy are defined by the Navier stokes equations and resolved in a Cartesian coordinate system as mentioned above. The origin of this system corresponds to the center of the base of the chimney at ground level as illustrated in Figure 1, with x in the direction of flow, y in the transverse direction and z in the span direction.

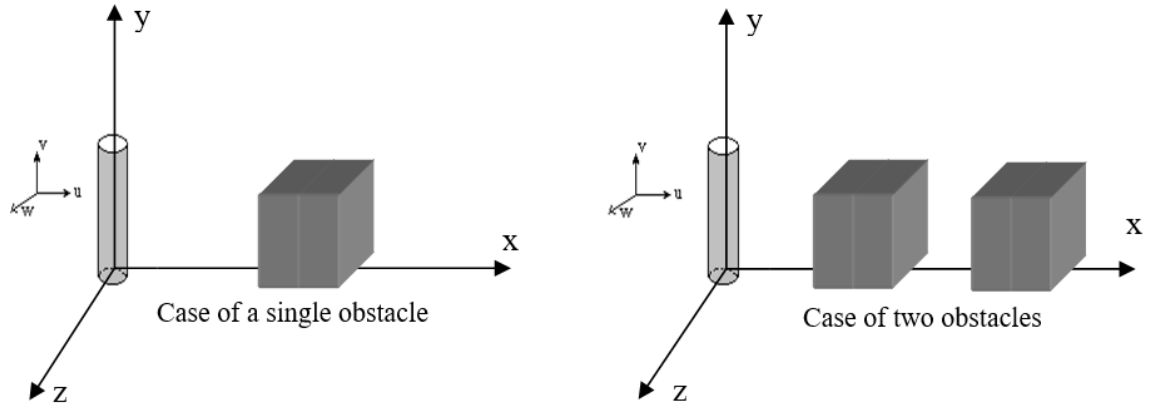

Figure 1. Schematization of the domain and definition of the coordinate axes.

The treated equations guiding this matter are obtainable using Favre's decomposition and are expressed in this case as follows:

Continuity equation:

$$\frac{\partial (\overline{\rho}\,\widetilde{u}_i)}{\partial x_i} = 0 \tag{1}$$

Momentum equations:

$$\frac{\partial (\overline{\rho}\,\widetilde{u}_j\,\widetilde{u}_i)}{\partial x_j} = -\frac{\partial \overline{p}}{\partial x_i} + \frac{\partial}{\partial x_j}\left(\mu\ \frac{\partial \widetilde{u}_i}{\partial x_j} - \overline{\rho u_i'' u_j''}\right) + \left(\overline{\rho}_\infty - \overline{\rho}\ \right) g_i \tag{2}$$

Energy equation:

$$\frac{\partial (\overline{\rho}\,\widetilde{u}_j\,\widetilde{T})}{\partial x_j} = \frac{\partial}{\partial x_j}\left[\ \left(\frac{\mu}{Pr} + \frac{\mu_t}{\sigma_t}\right)\frac{\partial \widetilde{T}}{\partial x_j}\right] \tag{3}$$

Mass fraction equation:

$$\frac{\partial (\overline{\rho}\,\widetilde{u}_j\,\tilde{f})}{\partial x_j} = \frac{\partial}{\partial x_j}\left[\left(\frac{\mu}{Sc} + \frac{\mu_t}{\sigma_f}\right)\frac{\partial \tilde{f}}{\partial x_j}\right] \tag{4}$$

The addition of fluctuating sizes makes this system open. Its closure needs the introduction of a turbulence model which allows getting a number of equations equivalent to the number of unknown variables.

The choice of a turbulence model strongly affects the accuracy of dispersion predictions around buildings because it greatly impacts the reproduction of the flow structure around buildings. However, this problem has not been adequately addressed since most previous studies have adopted the standard k- ε model and the LES model. Mahjoub et al. [19, 20] have shown that the three first-order models yield identical results in the upstream and downstream regions of the three-dimensional pollutant

stream ejection. But only the second-order model gives satisfactory results in the exit region and in the trailing area of the pollutant jet. It follows that the RSM model is beneficial in solving the system of equations described above. This benefit actually results from the capacity of the RSM model to predict the destruction of turbulence due to the dissipation rate of turbulent kinetic energy. It also includes further information about turbulent forces such as their anisotropy than other simpler approaches because it considers the generation of each of the Reynolds stress terms independently.

On the basis of this result, the second-order closure model is selected for the present study. The following equation is therefore solved:

$$\frac{\partial}{\partial x_k}\left(\overline{\rho}\,\tilde{u}_k\overline{u_i^{''}u_j^{''}}\right) = P_{ij} + G_{ij} + D_{ij} - \varepsilon_{ij} \tag{5}$$

Production term: $P_{ij} = -\overline{\rho}\,\left[\overline{u_i^{''}u_k^{''}}\frac{\partial \tilde{u}_j}{\partial x_k} + \overline{u_j^{''}u_k^{''}}\frac{\partial \tilde{u}_i}{\partial x_k}\right]$

Pressure strain correction: $G_{ij} = \overline{p'\left(\frac{\partial u_i^{''}}{\partial x_j} + \frac{\partial u_j^{''}}{\partial x_i}\right)}$

Diffusion term: $D_{ij} = \frac{\partial}{\partial x_k}\left[\mu\frac{\partial}{\partial x_k}\left(\overline{u_i^{''}u_j^{''}}\right) - \overline{\rho u_k^{''}u_i^{''}u_j^{''}}\right]$

Dissipation term: $\varepsilon_{ij} = 2\mu\left[\frac{\partial u_i^{''}}{\partial x_k}\frac{\partial u_j^{''}}{\partial x_k}\right]$

The equation depicting the turbulent kinetic energy and the dissipation rate of the kinetic energy related to the second-order model are described as below:

$$\frac{\partial\,(\overline{\rho}\,\tilde{u}_j\,k)}{\partial\,x_j} = \frac{\partial}{\partial\,x_j}\left[\left(\mu + \frac{\mu_t}{\sigma_k}\right)\frac{\partial\,\mathrm{k}}{\partial\,\mathrm{x}_j}\right] - \overline{u_i^{''}u_j^{''}}\frac{\partial \tilde{u}_i}{\partial x_j} - \overline{\rho}\,\varepsilon \tag{6}$$

$$\frac{\partial\,(\overline{\rho}\,\tilde{u}_j\,\varepsilon)}{\partial\,x_j} = \frac{\partial}{\partial\,x_j}\left[\left(\mu + \frac{\mu_t}{\sigma_\varepsilon}\right)\frac{\partial\,\varepsilon}{\partial\,\mathrm{x}_j}\right] - C_{\varepsilon 1}\frac{\varepsilon}{k}\left(\overline{u_i^{''}u_j^{''}}\frac{\partial \tilde{u}_i}{\partial x_j}\right) - C_{\varepsilon 2}\,\overline{\rho}\,\frac{\varepsilon^2}{k} \tag{7}$$

$$\boldsymbol{\mu_t = C_\mu\,\overline{\rho}\,\frac{\varepsilon^2}{k}}$$

The constants used are given in Table 1.

Table 1: Constants of the Turbulent Kinetic Energy and Dissipation Equations

$C_{\varepsilon 1}$	$C_{\varepsilon 2}$	σ_k	σ_ε
1.44	1.92	0.82	1.00

For further details about the constants inserted in the various equations, refer to the reference [14]. The boundary conditions combined with the system of differential equations outlined above are listed in Table 2.

Table 2. Boundary and emission conditions of the problem.

Boundaries	Velocity (m/s)	Temperature (K)	Mass Fraction	Kinetic energy m^2/s^2	Rate of dissipation $m^2\ s^{-3}$
Chimney outlet	$\tilde{u} = u_0,\ \tilde{v} = 0,\ \tilde{w} = 0$	$\tilde{T} = T_0$	$\tilde{f} = f_0$	$k_0 = 10^{-3} u_0^2$	$\varepsilon = k_0^{3/2} / 0.5d$ [23]
Transversal flow : wind	$\tilde{u} = u_\infty,\ \tilde{v} = 0,\ \tilde{w} = 0$	$\tilde{T} = T_\infty$	$\tilde{f} = 0$	$k_\infty = 510^{-3} u_\infty^2$	$\varepsilon = k_\infty^{3/2} / 0.2H_T$ [23] H_T represents the height of the computational domain.
Chimney wall, obstacle faces and ground	$\tilde{u} = 0,\ \tilde{v} = 0,\ \tilde{w} = 0$	$\frac{\partial \tilde{T}}{\partial n} = 0$	$\frac{\partial \tilde{f}}{\partial n} = 0$	$k = 0$	$\frac{\partial \varepsilon}{\partial y} = 0$
Domain limiting face	$\frac{\partial \tilde{u}}{\partial n} = 0,\ \frac{\partial \tilde{v}}{\partial n} = 0,\ \frac{\partial \tilde{w}}{\partial n} = 0$	$\frac{\partial \tilde{T}}{\partial n} = 0$	$\frac{\partial \tilde{f}}{\partial n} = 0$	$\frac{\partial k}{\partial n} = 0$	$\frac{\partial \varepsilon}{\partial n} = 0$

There are several significant issues arising from the numerical calculation of this task. The flow topology needs a very fine mesh in a large part of the domain. To accurately capture all parameter variations, particularly in the vicinity of the chimney and the obstacles, a non-uniform mesh is employed, refined near the chimney, the obstacles, and the ground. ANSYS Fluent employs the finite volume method, with the solution of the governing equations based on the SIMPLER algorithm proposed by Patankar [24]. An implicit scheme is adopted to obtain the algebraic equations. The Gaussian elimination method combined with a sub-relaxation technique is used to solve the resulting tridiagonal matrix. The iterative process is terminated when the convergence criteria, given in (8), is satisfied. The variable H may represent u, v, T, f, or any other relevant quantities.

$$\left| \frac{H^{m+1} - H^m}{H^{m+1}} \right| \leq 10^{-5} \tag{8}$$

3. Results and discussion

Emissions into the atmosphere must not, therefore, generate pollutant concentrations higher than values tolerable by regulations. The study of the flows of thermal plumes from chimneys is an essential point in the prevention of atmospheric pollution due to the operation of industrial plants, which are the

source of smoke and hot air emissions. The evolution of combustion products, coming from a chimney, conditions the spatial distribution of the more dangerous fumes. These products are a perfect illustration of the ecological dangers on man and the natural balance. Indeed, the analysis of the plumes observed at the exit of industrial chimneys can help in the development of prevention and safety techniques in relation to the atmospheric nuisances resulting from the penetration of these plumes into the environment.

The physical parameters that characterize the behavior of the effluent at the stack outlet are as follows:

- The diameter of the stack
- Ejection speed
- Wind velocity at the top of the chimney
- The relative temperature variation between the effluent and the ambient atmosphere.

The interest of air pollution modeling is to develop a quantitative relationship between the causes (industrial emissions) and the consequences (effects on health, heritage, ecosystems) of this pollution. The transport and dispersion of air pollution depends on the hydrodynamic and thermal conditions of the atmosphere, the quantitative and qualitative characteristics of the discharge and the local configuration of the land.

The results are obtained for uniform velocity and temperature profiles at the exit of the chimney, by varying the chimney height (h=57m, 85m, 114m) and the velocity ratio (R = 0.1, 0.5, 1, 2). A complete study of the influence of each of the physical parameters that characterize the behavior of the effluent at the chimney outlet leads to a very large number of cases to be analyzed. In order to present a reasonable quantity of solutions while identifying the essential physics of the problem, some parameters have been set. Thus, for this study, the results were obtained for different values of the velocity ratio R and a temperature difference equal to 92°C. By treating the evolution of the smoke composition, it was found that all species of smoke (CO_2, N_2, O_2, SO_2) have the same behavior: it is for this reason that carbon dioxide CO_2 was chosen as the study reference.

When a pollutant passes over an obstacle, several scales of turbulence can be registered. Near the source, it is the scales of the incident flow that induce the pollutant dispersion. Once the flow interacts with the building, this latter determines the scales of turbulence resulting from the detachment of the streamlines. In this section, the influence of various parameters such as wind velocity, smoke ejection velocity, chimney height and the location of obstacles relative to the chimney position on plume behavior was investigated. The levels of pollution on the ground and in buildings depend on the nature

and conditions of pollutant release, as well as the atmospheric conditions that determine the transport, diffusion and fallout of these same pollutants. The various parametric studies realized within the context of this present work are carried out in the case of a cubic-shaped building (Figure 1), the most general one, whose edge h_b is equal to 46 m. The spacing between the obstacles, L_2, and the position of the first building relative to the chimney, L_1, are kept fixed. The values L_1 = 114 m and L_2 = 92 m are adopted in the simulations.

3.1. Case of an isolated obstacle

The study of the dispersion of a pollutant requires, first of all, a good understanding of the flow behavior in the presence of the obstacle. Indeed, the extended recirculation zone, the nature of the sheared layer, as well as the nature of the vortices that detach from the obstacle, will interfere with the pollutant and thus affect its dispersion. The obstacles encountered by the flow often have a sharp-edged limit which amplifies instabilities. The detachment of the streamlines is abrupt, the wake is wider and the recirculation is more important. All these elements have a great influence on the accumulation and diffusion of the pollutant.

Figures 2 and 3 show the contours of the carbon dioxide mass fraction around the obstacle for different velocity ratios (R = 0.1, 0.5, 1, 2) and different chimney heights (h = 57m and 114m). It can be observed in Figure 2 that the pollutant streams tend to follow approximately the shape of the building, the latter generating a zone of ascent of the contaminant on its front face, followed by a zone of descent. The gaseous effluents emitted by the source are trapped in the stagnation zone and then convected towards the region downstream of the obstacle. Several observations made on the chimneys show that the fallout of the pollutants at ground level and on the obstacles in general is much greater when the chimney is low, which is confirmed by Figure 2.

In Figure 3, for a chimney height of h = 114m, the pollutant dispersion is observed to occur far from the buildings. This confirms the usual rule used to determine the right height of a chimney in order to have no encounter between the pollutant and the close wake, which recommends a chimney height equivalent to two and a half times that of the neighboring buildings, so as to avoid the fall back of the smoke. If this is not the case, the pollutant is entrained in the dead fluid area causing high concentrations on the rear side of the building. It is clear that the height of the chimney has a great influence on the diffusion and concentration of the pollutants on the ground and around the building.

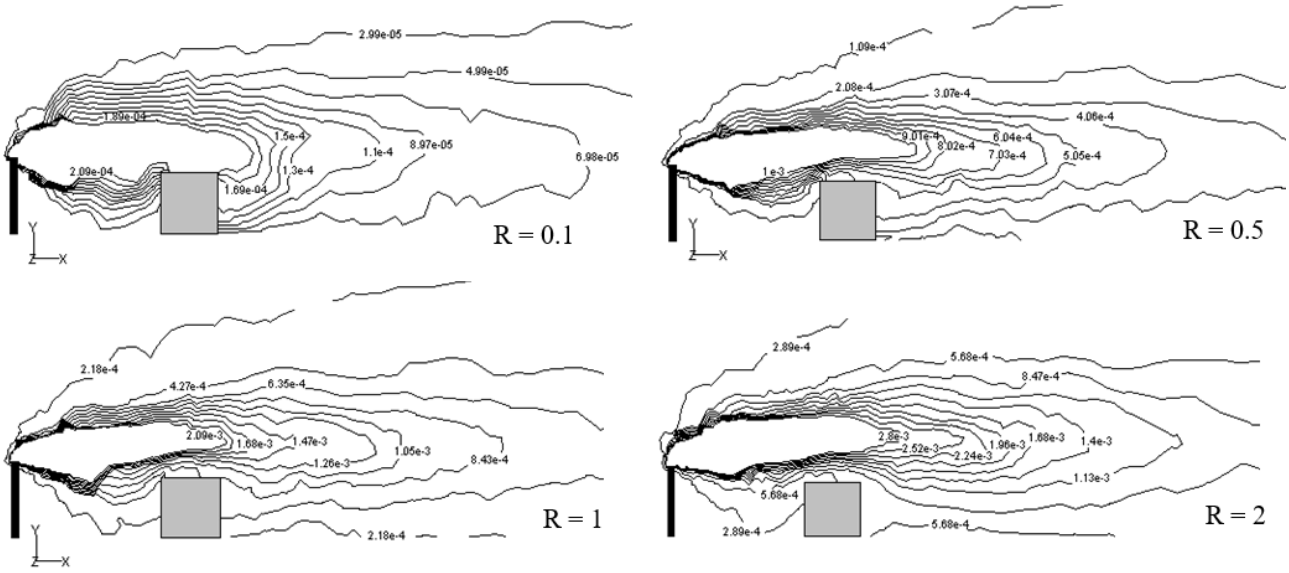

Figure 2. Contours of carbon dioxide mass fraction at a chimney height h = 57 m, under various speed ratios R, in the plan of symmetry z = 0

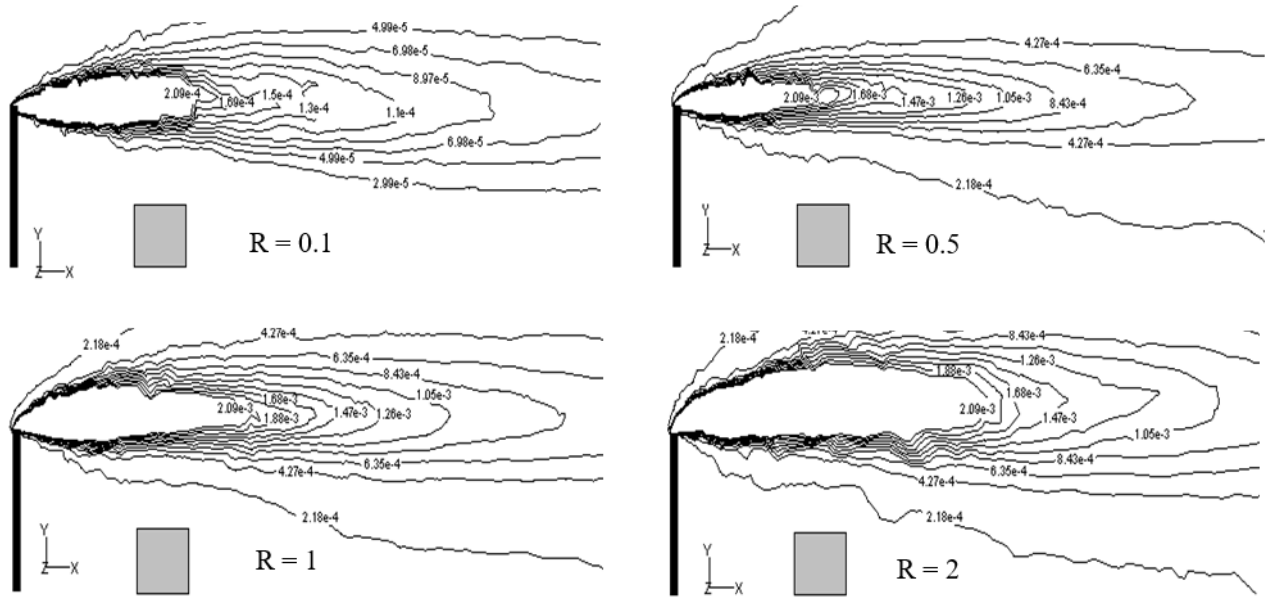

Figure 3: Contours of carbon dioxide mass fraction at a chimney height h = 114 m, under various speed ratios R, in the plan of symmetry z = 0

In Figure 4, the influence of the velocity ratio R (R = 0.1, 0. 5, 1, 2) on the Carbone dioxide mass fraction is examined for a fixed chimney height (h = 114 m). The analysis is carried out at several streamwise sections: upstream of the obstacle (x = 50 m and 100 m), at the front edge (x = 115 m), at mid-roof level (x = 137 m), at the rear edge (x = 159 m), and further downstream (x = 200 m and 400

m). This figure indicates that the stronger the wind speed, the greater the dispersion of pollutants is (R = 0.1). Indeed, in this case, the air flow due to the wind is sufficiently important to provide higher dilution of the pollutant. For a speed ratio R = 2, the mass fraction is greater than that obtained when this ratio is equal to 0.1.

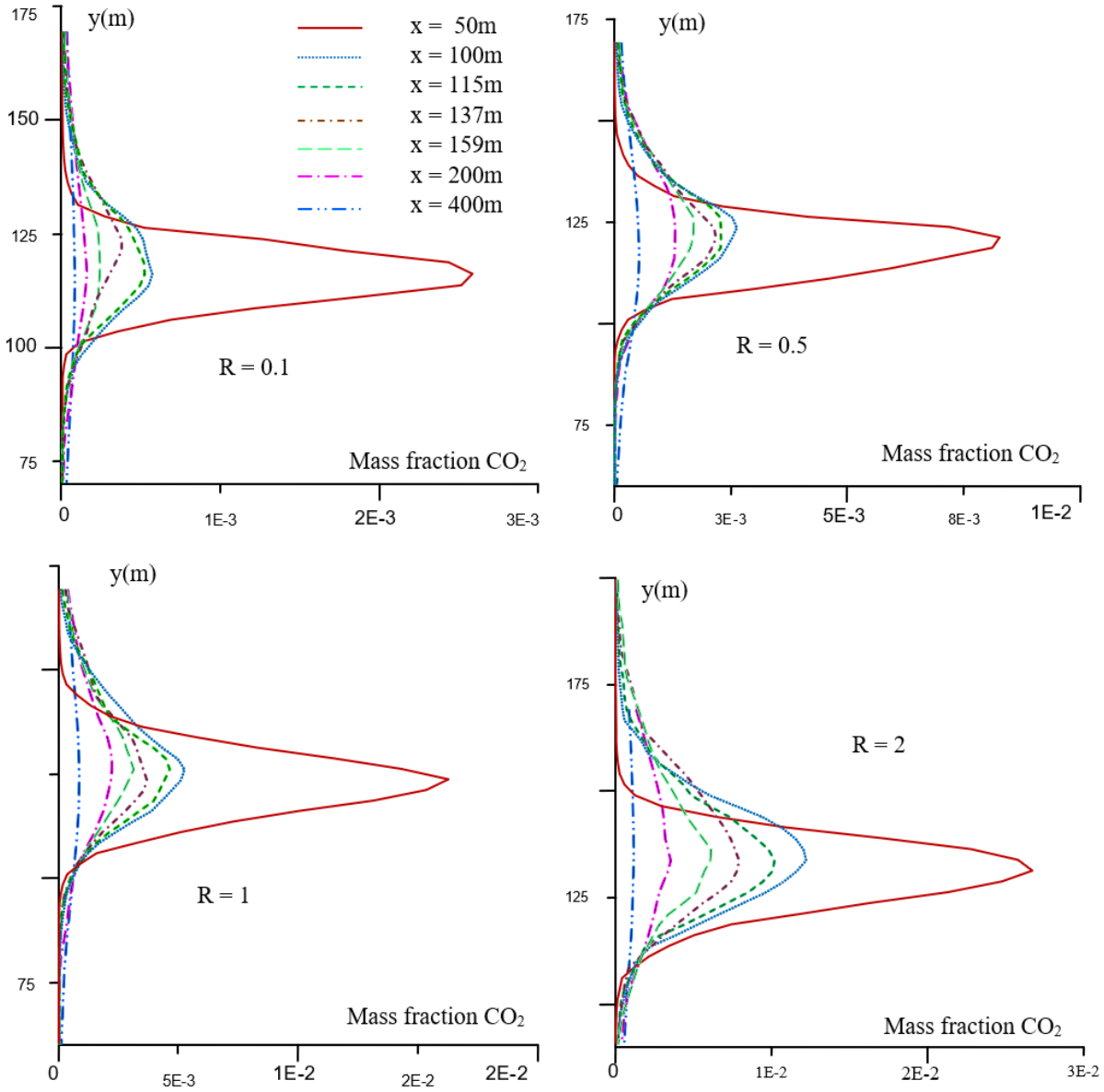

Figure 4: Evolution of the mass fraction of CO_2 in different sections along the flow for a height h = 114 m (case of a single building)

Figure 5 shows the evolution of the longitudinal velocity as a function of y, normal coordinate, in different longitudinal sections of the flow for a chimney height h = 114 m. A flow disturbance due to building obstruction can be seen. For x = 100 m, a return fluid is observed at a reduced height. It is clear that on the downstream of the building (x = 400 m), the evolution of the longitudinal velocity is

regular and does not depend practically any more on the presence of the obstacle, the latter having no effect on the flow.

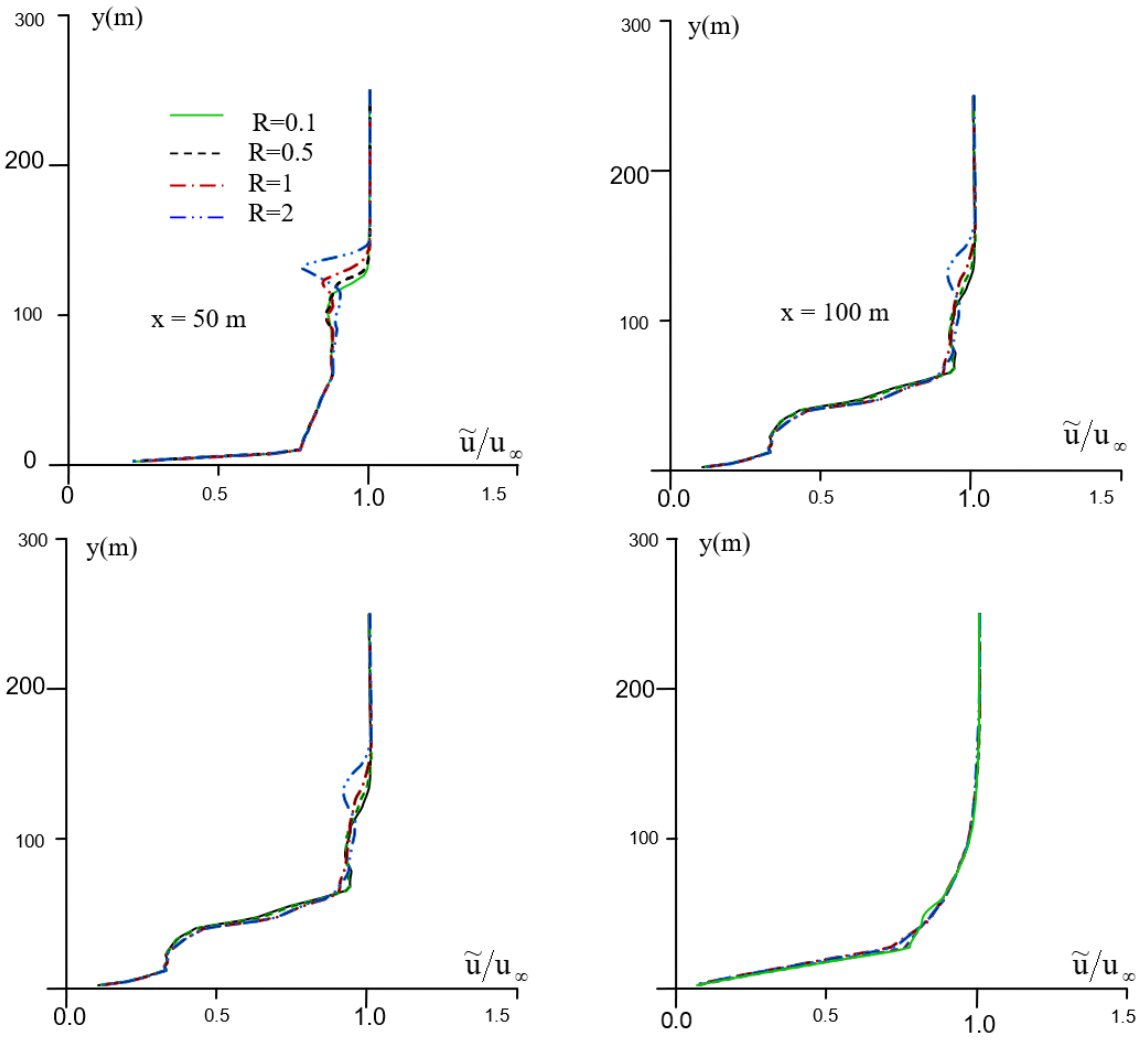

Figure 5: Evolution of the longitudinal speed ratio $\tilde{u}/u_\infty$ for different velocity ratios R at a height h = 114 m

In Figure 6, the profiles of the mass fraction are presented for different velocity ratios R and for a chimney height of h =57 m. The evolution of the pollutant before the obstacle and in the surroundings of the building is examined. For the area between the chimney and the obstacle, the concentration of the pollutant is minimal and this is valid for the four velocity ratios used. On the front face, it can be seen that the lowest mass fraction is that obtained for a velocity ratio R = 2, i.e. in the case where the ejection velocity is the highest. In this region, the plume, still in its first phase of evolution, is guided by its initial inertia.

On the roof and on the rear face, the maximum mass fraction is observed for a velocity ratio R= 1, corresponding to a situation in which the ejection velocity is of the same order of magnitude as the

wind velocity. Regardless of the velocity ratio, the largest mass fraction is observed at the roof, on the downstream edge and on the rear face at ground level where the pollutants are trapped.

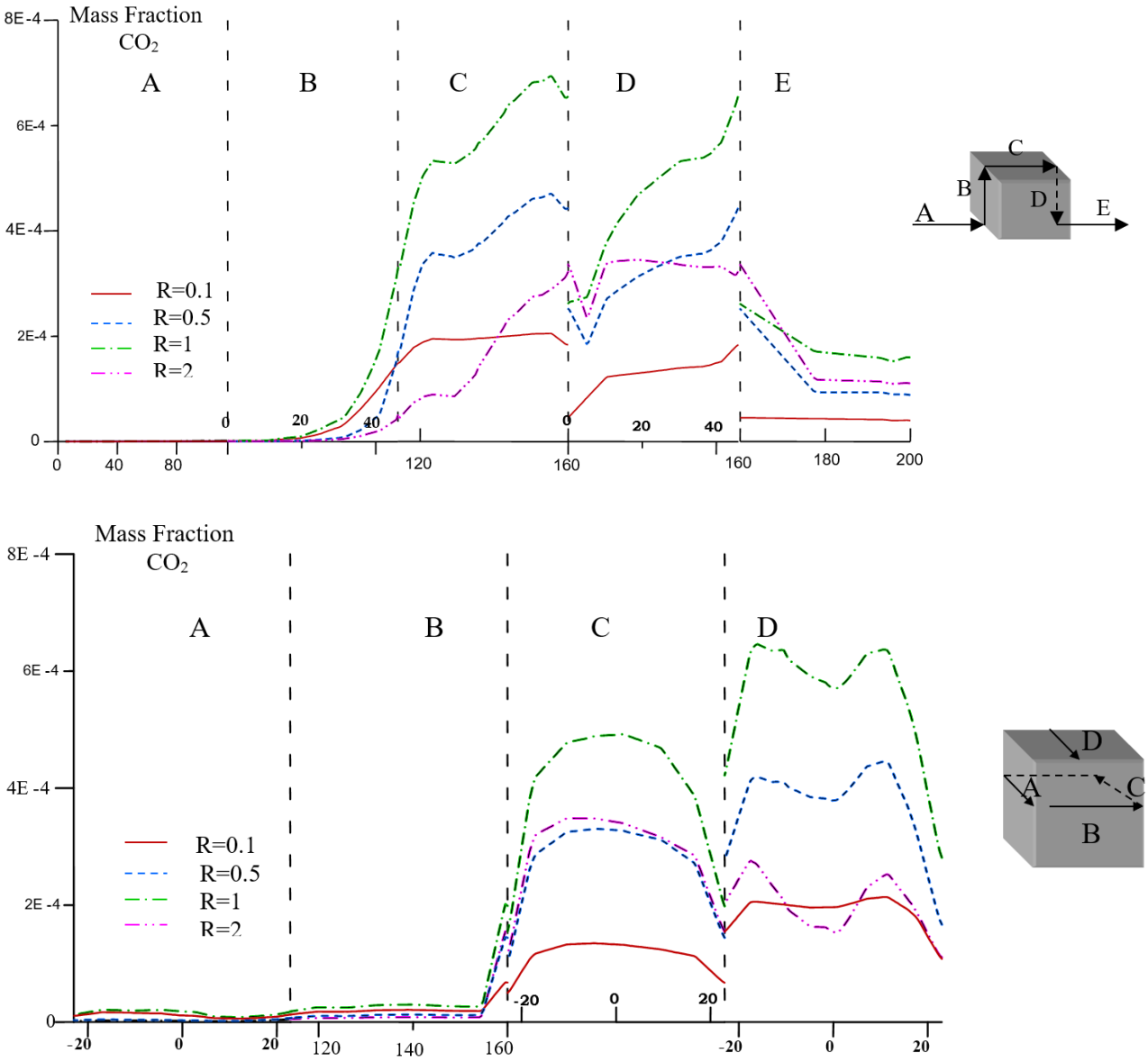

Figure 6: Evolution of CO_2 mass fraction on the ground and on the building faces for different speed ratios R and a height h = 57 m

In Figure 7, the lateral distribution (along z) of the vertical velocity ($\tilde{v}$) is presented for different longitudinal positions (along x) along the plume evolution, at roof level (y = 46 m), for a velocity ratio R = 0.5. At x = 100 m, the vertical velocity is higher than at x = 50 m. For x = 115 m, the flow is slowed down by the presence of the obstacle. The profile, in this section, has two peaks because the flow wraps around the obstacle and envelops the front face. These peaks attenuate as x (longitudinal

coordinate) increases. The negative velocity indicates recirculation zones (for x = 200m). For x = 400m, there is practically no recirculation.

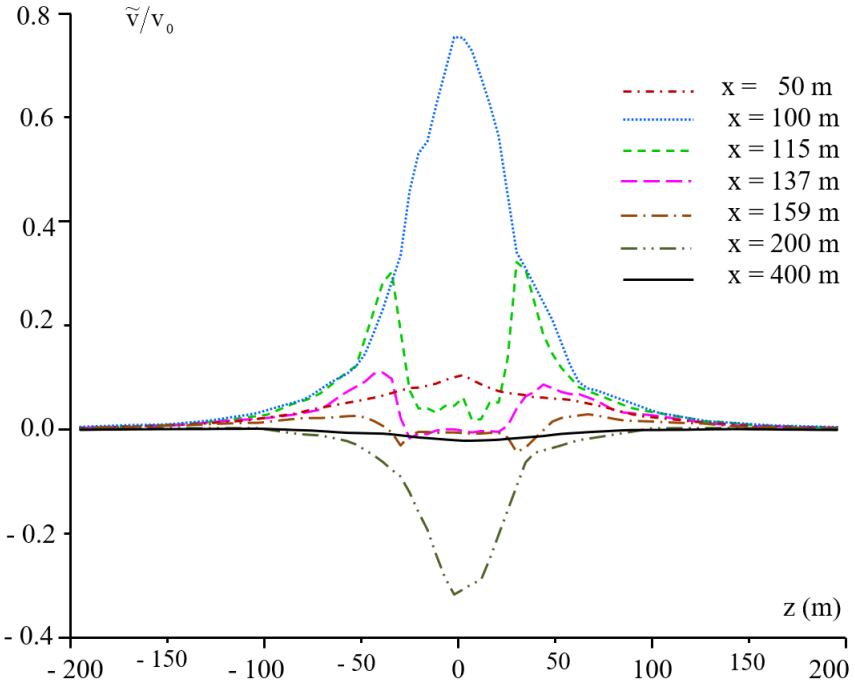

Figure 7: Evolution of the vertical velocity ratio $\tilde{v}/v_0$ for R = 0.5 at a height h = 57 m

3.2. Case of two obstacles

It can be seen from Figure 8, where the contours of the carbon dioxide mass fraction around two obstacles are given, that when the polluted air encounters obstacles, its flow is disrupted and some streams bypass the obstacles in front of them while others tend to cross them. The iso-concentrations are tightened over rooftops and between obstacles, creating strong shear forces, and then become more regular downstream, away from the obstacles. The pollutant is affected by the average flow around the primary obstacle by recirculation zones, wakes and turbulence generated in these zones. The second obstacle building only rises the disturbance of the pollutant flow in the mixing layer.

Figure 9 shows the profiles of the CO_2 mass fraction as a function of y (normal coordinate) for different longitudinal positions along the flow in the symmetry plane (z = 0). The higher the velocity ratio R, the more the position of the maximum of the mass fraction moves upwards for all considered sections with an increasing in its value.

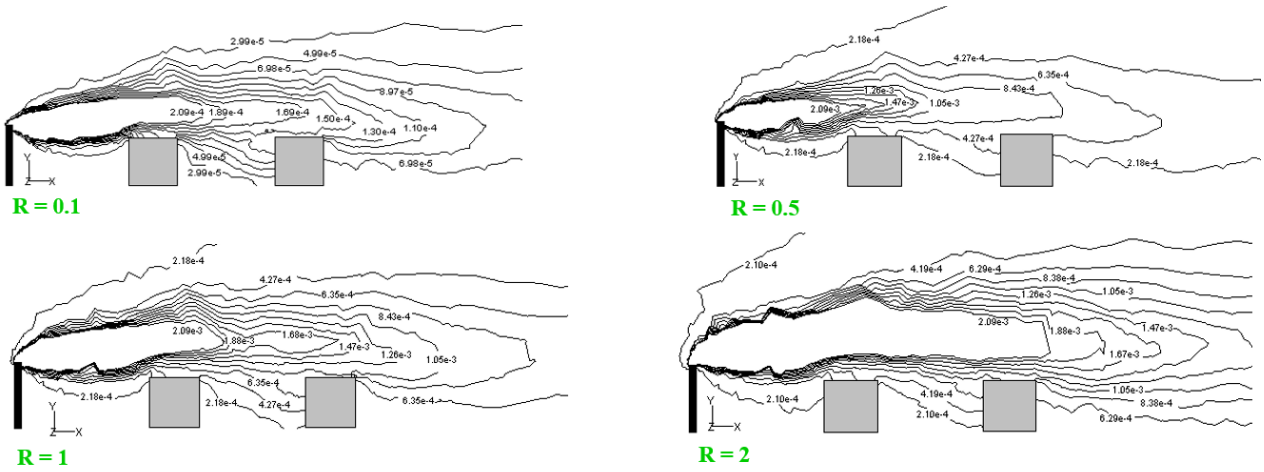

Figure 8: Contours of mass fraction of carbon dioxide around two obstacles at a chimney height h = 57 m (in the plane of symmetry)

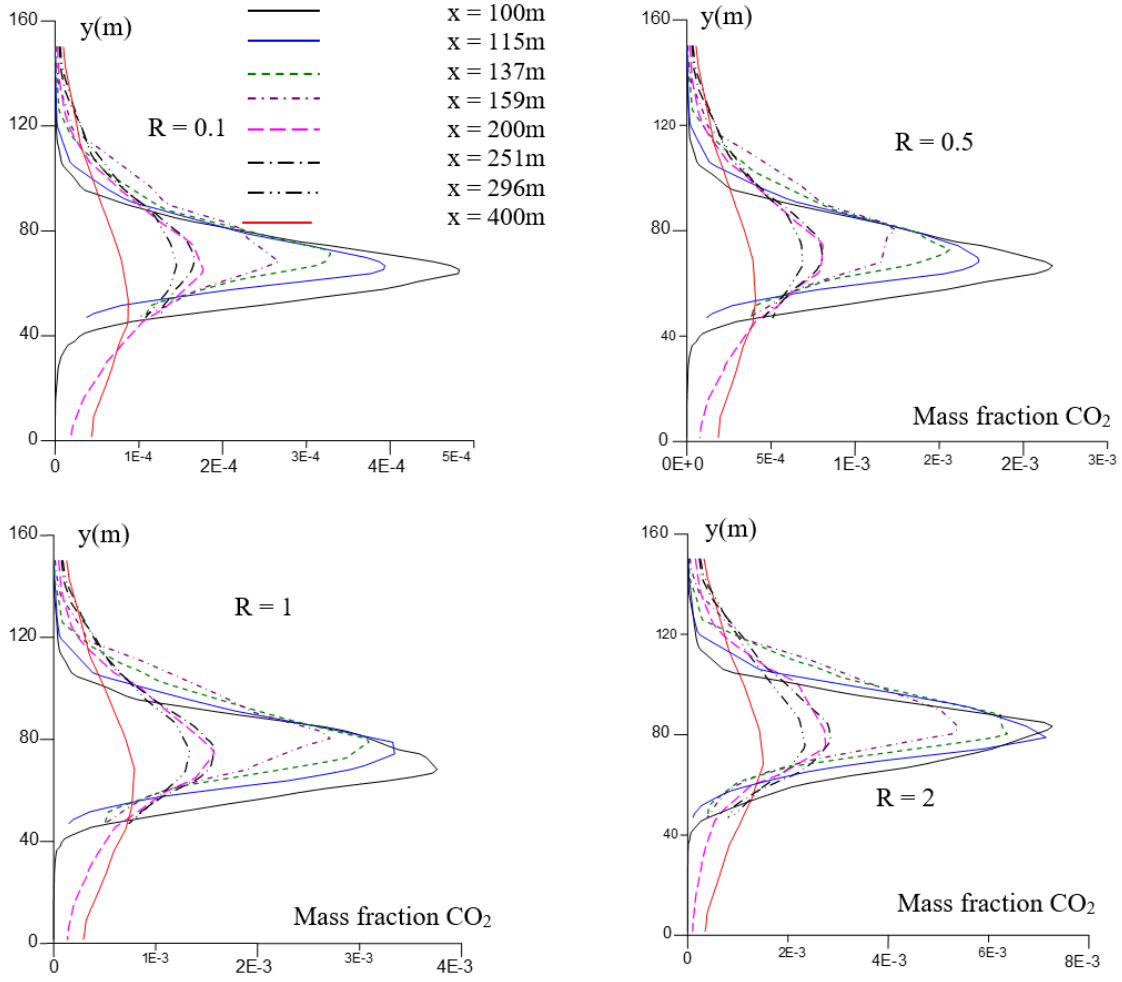

Figure 9: Evolution of CO_2 mass fraction in different sections along the flow for a height h=57m (case of two buildings, z = 0)

In Figure 10, the mass fraction profiles around the obstacles are presented for a chimney height of h=57m, and for different velocity ratios R (R = 0.1, 0. 5, 1, 2). It can be seen that for the first hundred meters downstream of the chimney and at ground level, the mass fraction is very low. On the front face (B), the fraction of pollutant is low compared to that of the roof (C) where a sharp increase can be observed. The structure of the flow between the two obstacles (D, E, F) is complex and the transfers with the external flow are more intense. There are several wake zones resulting from the disturbances caused by the two obstacles. The pollutant drops on the second obstacle and, as a result, the mass fraction is maximal on the roof of the second obstacle (G). In this region H, there is a significant return of pollutant due to a recirculation zone which is very important on the back side of the second building: the pollutant is then trapped and a significant concentration is observed, although lower than that of the roof. Downstream of the second obstacle, the resistance of the buildings disappears. In his study, Alvares [25] also noted this process. It should also be noted the strong vortex activity above the two obstacles, because of the presence of small turbulent structures that govern the vertical transfer.

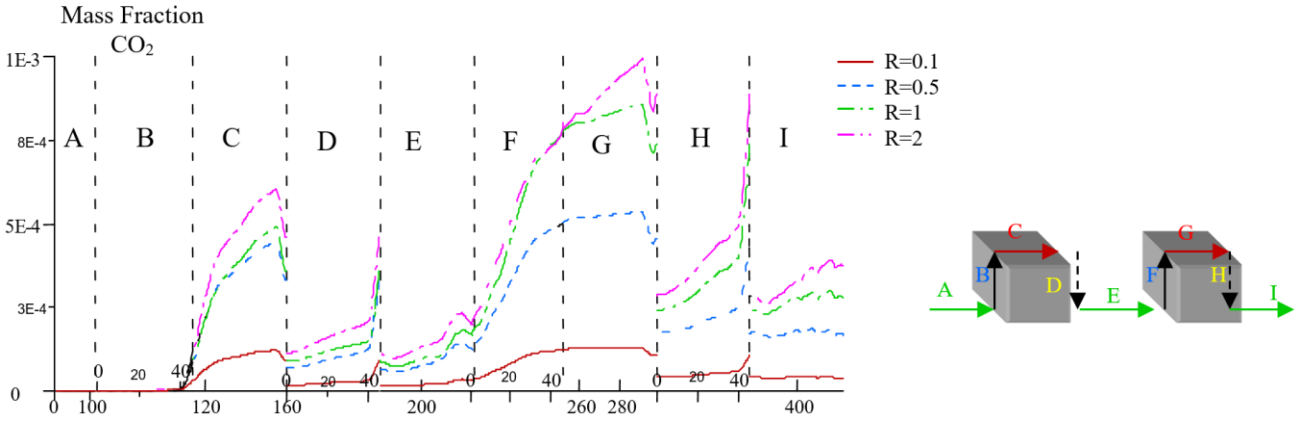

Figure 10: Evolution of the mass fraction of CO_2 on the ground and on buildings faces for different speed ratios R and chimney height h = 57 m

In order to highlight the acceleration of the fluid imposed by the contouring of obstacles and to characterize the area of vortex formation, cartography of the velocity vectors is presented in Figure 11. It can be seen that the gas emitted by the chimney bypasses the first obstacle and follows its geometry. When the pollutant hits obstacles distant of L_2 and placed at a distance L_1 from the chimney, the perturbation is consequent and it is easy to distinguish four main zones interposed between the mean flow and the two buildings. Zone 1 is created by the return movement of the fluid at its impact on the first building. Zone 2 is situated on top of the former building. The sudden increase in pressure caused by the first building causes the fluid to deflect towards the space above this building. The zone 3 is

determined by the gap between the two obstacles which contains a mass of fluid driven in a vortex movement of considerable size. In addition, other recirculations, of much smaller dimensions than the first one and evolving downstream of the first building and upstream of the second, also exist in this region. Finally, Zone 4 is the downstream region of the second building. This zone is created due to the impact of the second building. The dimensions of this zone increase with velocity.

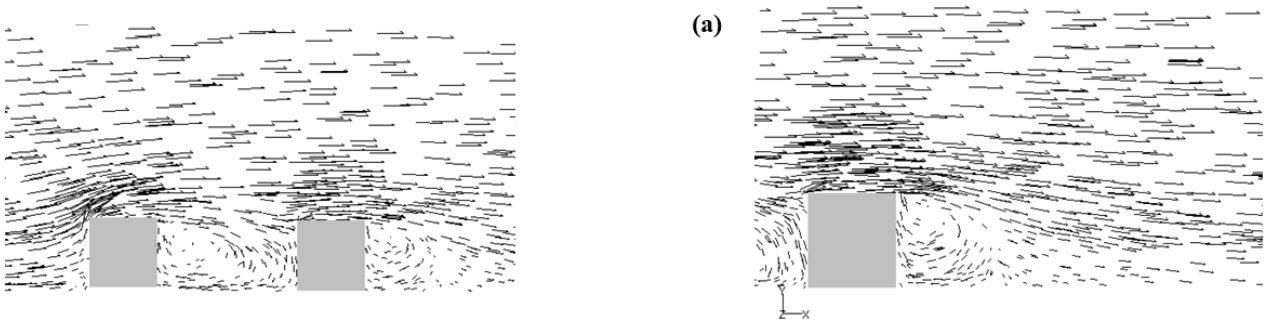

Figure 11: Distribution of velocity vectors for the case of two buildings, in the plane of symmetry, for a height h = 85 m and a speed ratio R = 2 **(a)** Zoom of the area behind the second building.

Figures 12 and 13 present the distribution of the CO_2 mass fraction on the ground and on the buildings faces for two geometrical configurations of the obstacles relative to the chimney, with a chimney height of h = 85 m and a velocity ratio R = 2. The first configuration (Figure 12) is designed with two obstacles on the same level and located at a distance of 114 m from the chimney. In the second configuration (figure 13), the two buildings are on the same side and at a distance of 114 m from the chimney. It can be seen that when the buildings are displaced with regard to the chimney, the rate of pollutant deposited on the ground and on the buildings is lower by a factor of 3.2 than that deposited when the buildings are located in the axis of the chimney.

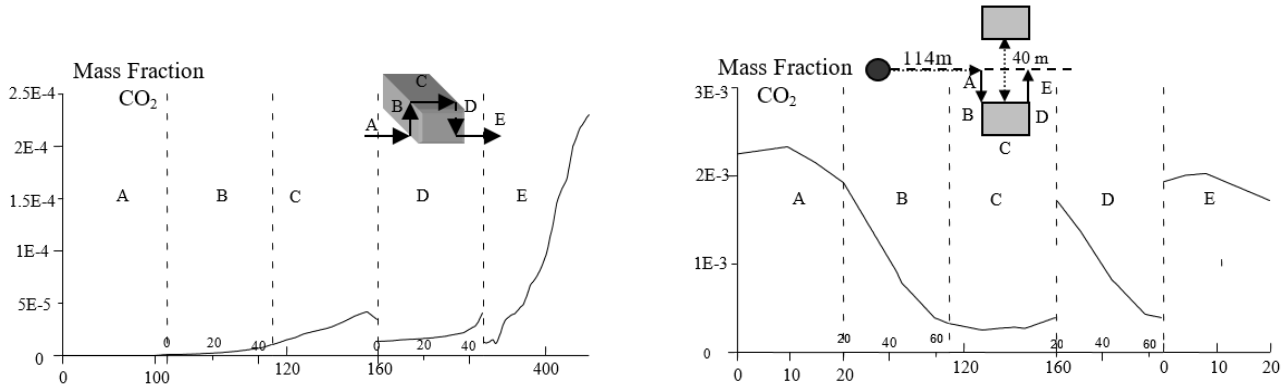

Figure 12: Evolution of CO_2 mass fraction on the ground and on the buildings faces in the same position with regards to the chimney and at a distance of 40m, for a height h = 85 m and R = 2.

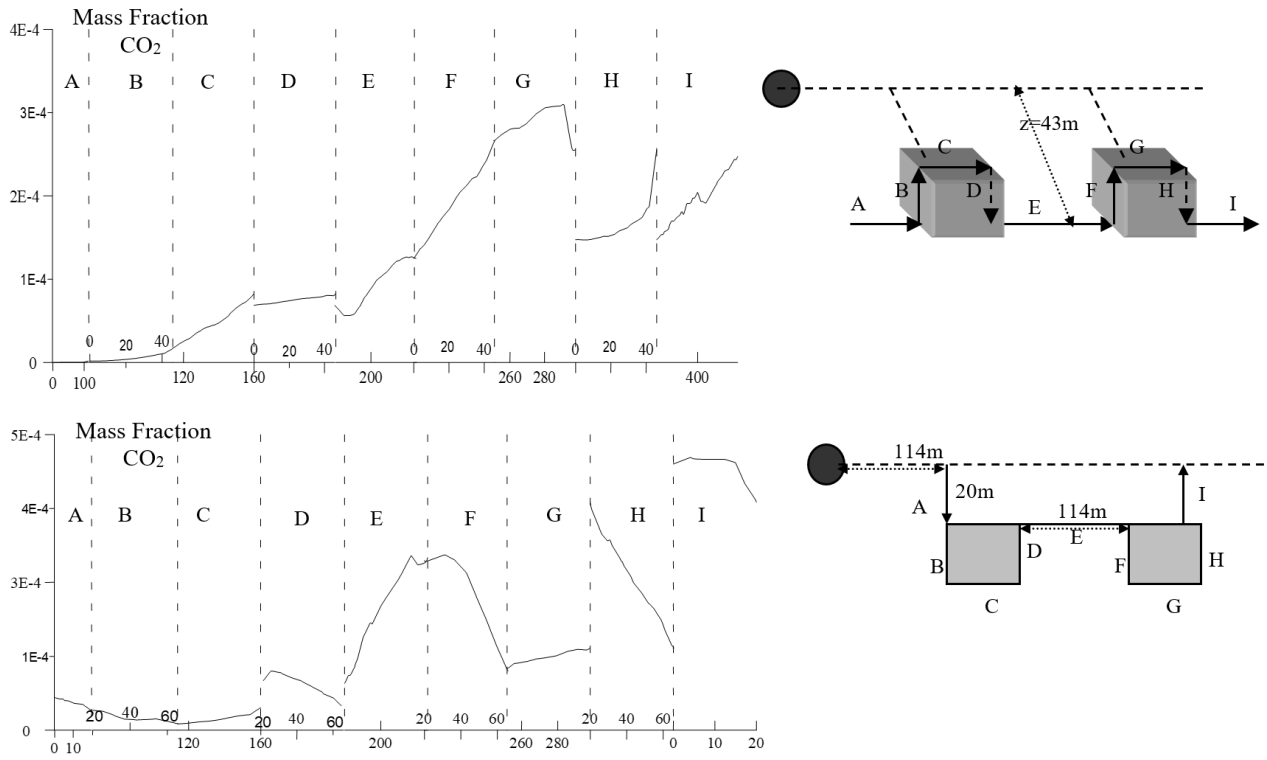

Figure 13: Evolution of CO_2 mass fraction on the ground and on the buildings faces on the same side, at 20m from the median plane, for a height h = 85 m, R = 2.

The distributions of the velocity vectors around the two buildings as a function of their relative position to each other and to the chimney are shown in Figure 14 for R = 2, at the plane y = 23 m and for a height h = 85 m. This figure gives an idea of the flow structure. The depression and recirculation zones behind the obstacles where the pollutants are trapped are clearly visible. It can be noticed that the flow decelerates when approaching the obstacle, whereas upstream there is a zone of fluid blockage. At the place where the flow arrives on the obstacle, a detachment of the sheared layer is formed which causes the appearance of a vortex. It is, indeed, the physical mechanism that is at the origin of what is called vortex escapement.

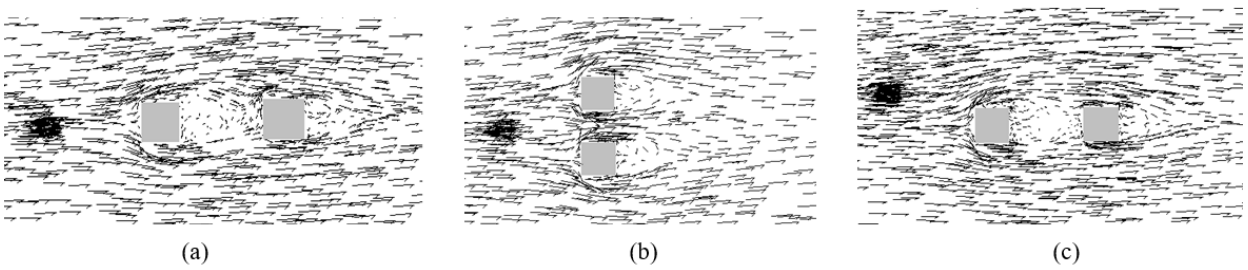

Figure 14: Distribution of velocity vectors, at the plan y = 23 m, around the two buildings as a function of their locations, for R = 2 and h = 85 m.

The previous results indicate that, when the buildings are widely spaced, the flow behaves similarly to a sequence of isolated structures around individual buildings. When the gap diminishes, the wakes are perturbed. The flow downstream of one building is intensified by a deviation at the upstream side of the next building. When the ratio (W/h_b) is even lower, the flow is referred to as grazing.

In order to confirm these observations, four configurations are considered:

- The two obstacles are spaced at a distance equal to four times the building height (Figure 15a).
- The two obstacles are spaced at a distance equal to twice the building height (Figure 15b).
- The two obstacles are spaced at a distance equal to the building height (Figure 15c).
- The two obstacles are spaced at a distance equal to half the building height (Figure 15d).

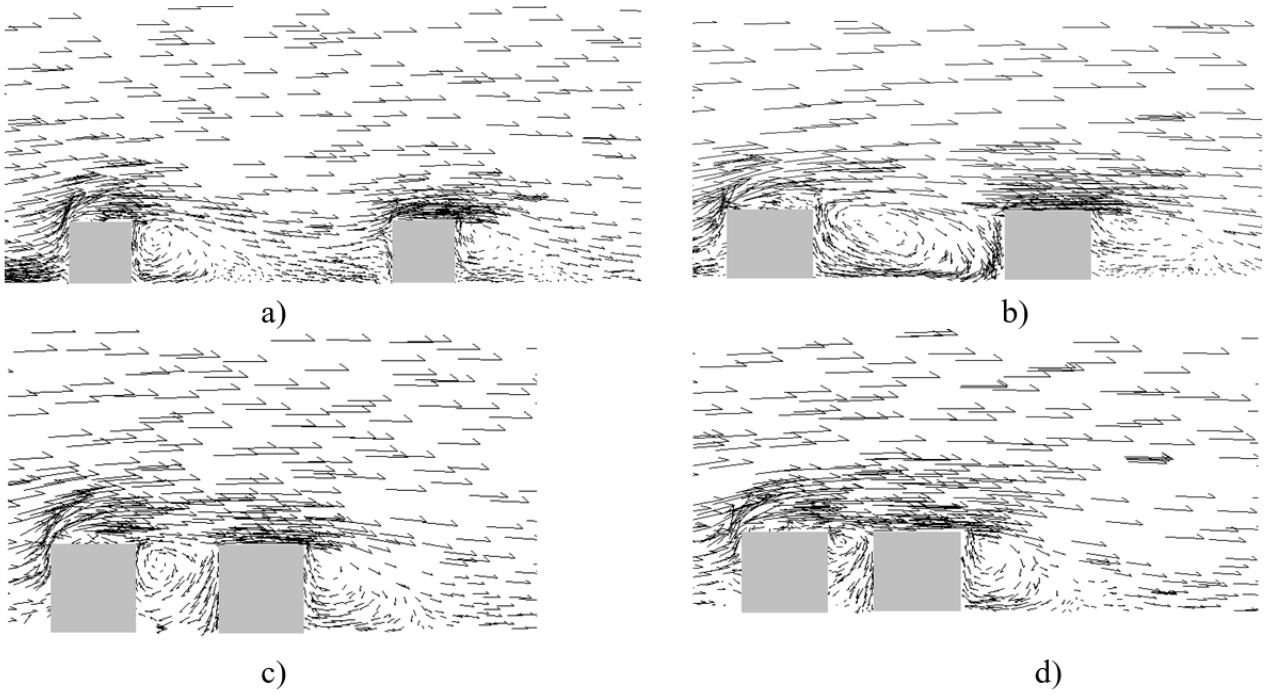

Figure 15: Distribution of velocity vectors for R=2 and h=57 m for different building spacings: (a) $W=4h_b$, (b) $W=2h_b$, (c) $W=1h_b$, (d) $W=0.5h_b$

In Figure 15a, the vortex originating from the top of the first building propagates downstream. It grows as it passes over the leeward face, with the vortex center initially moving closer to the ground. The flow then returns toward the building and collapses against the rear face before being carried downstream. In this configuration, the recirculation zone remains attached to the back face of the first obstacle, without influencing the second obstacle. This corresponds to a flow regime with isolated structures.

In the second configuration (Figure 15b), the flow exhibits a set of circulations both upstream and downstream of the obstacles. This configuration corresponds to a flow regime with disturbed structures.

In the third configuration (Figure 15c), large recirculation zones develop between the two obstacles, indicating strong interaction of the flow within the confined space.

In the fourth configuration (Figure 15d), the buildings are very close together, leading to a compact recirculation pattern primarily over the leeward side of the first obstacle and the front of the second obstacle. The third and fourth configurations correspond to the grazing flow regime.

Table 3 reports the maximum values of the carbon dioxide mass fraction observed in three regions: on the roof of the first obstacle, on the ground in the area separating the two obstacles, and on the roof of the second obstacle. As shown in Table 3, the third configuration ($W = h_b$) produces the highest pollutant concentrations across all regions. The absolute maximum mass fraction occurs on the roof of the second obstacle in this configuration (1.13×10^{-3}), indicating that pollutant trapping is most pronounced when the spacing between the buildings corresponds to $W = h_b$.

Table 3. Maximum CO_2 Mass Fraction Values for Four Building Spacing Configurations (W/h_b)

	Roof of the first obstacle	Between the two obstacles	Roof of the second obstacle
First configuration ($W = 4h_b$)	8.915×10^{-4}	2.51×10^{-4}	9.92×10^{-4}
Second configuration ($W=2h_b$)	5.274×10^{-4}	3.95×10^{-4}	1.28×10^{-4}
Third configuration ($W=h_b$)	9.61×10^{-4}	4.42×10^{-4}	1.13×10^{-3}
Fourth configuration ($W=1/2h_b$)	5.04×10^{-4}	2.38×10^{-4}	8.2×10^{-4}

4. Conclusion

The shape of the land and nearby structures plays a key role in how pollutants move and spread in the atmosphere. When a released pollutant meets obstacles, its path can bend sideways or upward, and swirling motions often appear behind those obstacles. In this work explores the influence of several factors, including wind speed, emission velocity, chimney height, and the position of nearby buildings, on pollutant dispersion in the air. The findings indicate that the chimney's height, compared to the surrounding buildings, has a strong impact on how pollutants travel. The effective release height also influences how much pollutant settles on rooftops, while higher wind speeds help spread the pollutants more widely. When multiple buildings are considered, fewer buildings located downwind of the chimney result in significantly lower pollutant levels at their height. Depending on the ratio between

building height and spacing (h_b/W), the airflow can follow one of the patterns described by Oke [26]: isolated roughness flow, wake interference flow, or skimming flow. Overall, these results highlight how important it is to consider the local landscape and building layout when planning industrial sites. Because each location has its own environmental and topographical features, simulations should be tailored to each case, taking into account terrain shape, surrounding structures, and local weather, to achieve safer and more efficient pollutant control.

References

[1] Tominaga Y., Stathopoulos T. (2009). Numerical simulation of dispersion around an isolated cubic building: comparison of various types of k-ε models, Atmos. Environ. 43 3200–3210.
[2] Tominaga Y., Stathopoulos T. (2010). Numerical simulation of dispersion around an isolated cubic building: model evaluation of RANS and LES, Build. Environ. 45 2231–2239.
[3] Gousseau P., Blocken B., van Heijst G.J.F. (2011). CFD simulation of pollutant dispersion around isolated buildings: on the role of convective and turbulent mass fluxes in the prediction accuracy, J. Hazard Mater. 194 422–434.
[4] Jiang Guoyi, Yoshie Ryuichiro (2020). Side ratio effects on flow and pollutant dispersion around an isolated high-rise building in a turbulent boundary layer, Building and Environment, Volume 180, August 107078
[5] Rossi, R., Philips, D.A., Iaccarino, G. (2010). A numerical study of scalar dispersion downstream of a wall-mounted cube using direct simulations and algebraic flux models. Int. J. Heat Fluid Flow 31, 805–819.
[6] Rossi R., Iaccarino G. (2013). Numerical analysis and modeling of plume meandering in passive scalar dispersion downstream of a wall-mounted cube, Int. J. Heat Fluid Flow 43 137–148.
[7] Yassin M.F., Alhajeri N.S., Elmi, A.A., Malek M.J., Shalash M. (2021). Numerical simulation of gas dispersion from rooftop stacks on buildings in urban environments under changes in atmospheric thermal stability. Environ Monit Assess 193, 22 https://doi.org/10.1007/s10661-020-08798-x
[8] Ben Ramoul L., Korichi A., Popa C., Zaidi H., Polidori G. (2019). Numerical study of flow characteristics and pollutant dispersion using three RANS turbulence closure models, Environmental Fluid Mechanics, 19, 379–400 https://doi.org/10.1007/s10652-018-9628-2
[9] Fu Y., Lin X., Li L., Chu Q., Liu H., Zheng X., Liu C.-H., Chen Z., Lin C., Tse T. K. T., Li C. Y. (2023). A POD-DMD augmented procedure to isolating dominant flow field features in a street canyon. Physics of Fluids, 35(025112).
[10] Fu Y., Lin X., Li L., Chu M., Liu C.-H., Chen Z., Li C. Y., Tse K. T. (2023). The NOx–O3 photochemical reactive air pollutant dispersion around an isolated building—the role of turbulence model and building aspect ratio. Building and Environment, 245, 110906.
[11] Huang X., Wang P., Song L., Bai Y., Zhang L., Gao L. (2024). Numerical simulation of airflow and pollutant dispersion around high-rise buildings with different rotation angles. Processes, 12, 2828.
[12] Chen W., Wang Z., Hong H., Song J., Hu G. (2025). Aerodynamic interference effects on three connected high-rise buildings with Y-plan layout. Engineering Structures, 326, 119494.
[13] Quentin F., Viet Duong D., Dinh Duc N. (2025). Numerical modeling of turbulent flows influencing the dispersion of atmospheric pollutants around a high-rise building in an urban environment. VNU Journal of Science: Mathematics – Physics. https://doi.org/10.25073/2588-1124/vnumap.5053

[14] Chavez Mauricio, Hajra Bodhisatta, Stathopoulos Ted, Bahloul Ali (2011). Near-field pollutant dispersion in the built environment by CFD and wind tunnel simulations, Journal of Wind Engineering and Industrial Aerodynamics, Volume 99, Issue 4, Pages 330-339
[15] Lateb Mohamed, Masson Christian, Stathopoulos Ted, Bédard Claude (2010). Numerical simulation of pollutant dispersion around a building complex, Building and Environment 45 1788-1798.
[16] Liu X. P., Niu J. L., Kwok K. C. S., Wang J. H., Li B. Z. (2010). Investigation of indoor air pollutant dispersion and cross-contamination around a typical high-rise residential building: Wind tunnel tests. Building and Environment, 45(8), 1769–1778. doi:10.1016/j.buildenv.2010.02.003
[17] Zhang Y., Kwok K.C., Liu X.P., Niu J.L., (2015). Characteristics of air pollutant dispersion around a high-rise building, Environ. Pollut. 204, 280–288
[18] Yu Y., Kwok K.C.S., Liu X.P., Zhang Y. (2017). Air pollutant dispersion around high-rise buildings under different angles of wind incidence, Journal of Wind Engineering & Industrial Aerodynamics 167 51–61
[19] Mahjoub Said N., Mhiri H., El Golli S., Le Palec G., Bournot P. (2003). Three-dimensional numerical calculations of a jet in an external cross flow: application of dispersion of pollutants, Journal of Heat Transfer. Transactions of the ASME, Vol. 125, p. 1-13.
[20] Mahjoub Said N., Mhiri H., Le Palec G., Bournot P. (2005). Experimental and numerical analysis of pollutant dispersion from a chimney, Atmospheric Environment, Vol. 39 pp. 1727-1738
[21] Mahjoub Said N., Mhiri H., Caminat P., Le Palec G., Bournot P. (2008). Wind tunnel investigation and numerical simulation of the near wake dynamics for rectangular obstacles, Environmental Engineering Science, Vol. 25, N°7, pp. 1037-1060,
[22] Mahjoub Said N., H. Mhiri, H. Bournot, G. Le Palec. (2008). Experimental and numerical modelling of the three-dimensional incompressible flow behaviour in the near wake of circular cylinders, Journal of Wind Engineering & Industrial Aerodynamics, Vol. 96, issue N°5, pp. 471-502
[23] Demuren, A.O., Rodi, W. (1987). Three Dimensional Numerical Calculations of Flow and Plume Spreading Past Cooling Towers", J. Heat Transfer, 109, pp. 113–119
[24] Patankar, S.V., D.B., Spalding, A calculation procedure for heat, mass and momentum transfer in three-dimensional parabolic flows, Int. J. Heat Mass Transf., 15, pp. 1787–1806, 1972.
[25] Alvares Levi S. (1993). simulation numérique des écoulements urbains à l'échelle d'une rue à l'aide d'un modèle k-ε. Thèse de doctorat, école centrale de Nantes
[26] Oke T.R. (1988). Street design and urban canopy layer climate. Energy and Buildings, vol. 11, p103-113.